Geodesy and Geodynamics 8 (2017) 77–83

Contents lists available at ScienceDirect

Geodesy and Geodynamics

journal homepages: www.keaipublishing.com/en/journals/geog;
http://www.jgg09.com/jweb_ddcl_en/EN/volumn/home.shtml

Quantitative analysis of the Nepal earthquake on 25 April, 2015 in the perspective of future earthquake hazard

Mallika Mullick*, Dhruba Mukhopadhyay

Raman Centre for Applied and Interdisciplinary Sciences, 16A, Jheel Road, Kolkata 700075, India

ARTICLE INFO

Article history:
Received 9 May 2016
Accepted 9 January 2017
Available online 22 February 2017

Keywords:
Nepal Himalaya
Aftershock
Positive Coulomb stress change
Co-seismic displacement
Future earthquake

ABSTRACT

The earthquake that occurred in Nepal on 25 April, 2015 was followed by about 256 aftershocks which continued for another 20–25 days. The Coulomb stress change due to the main shock has been estimated at depths 10 km, 15 km and 22 km which justify the occurrence of about 218 aftershocks of magnitudes 4 to 5 mostly at 10 km depth and the rest of magnitudes 5 to 7.3 mostly at 15–30 km depth. The western, southern and northern fringes of the fault plane that slipped on 25 April, 2015 show a high value of positive Coulomb stress change estimated at the above mentioned depths and yet these parts of the fault remained devoid of any aftershock epicentre and therefore must be treated as seats for possible future events. Co-seismic displacement of 5 GPS stations located in Nepal after the devastating earthquake of *M*w7.8 on 25 April, 2015 and its largest aftershock of *M*w7.3 on 12 May, 2015 have been separately estimated and analysed.

1. Introduction

On 25 April, 2015 an earthquake of *M*w7.8 occurred about 77 km northwest of Kathmandu in Nepal at a focal depth of 8.2 km (http://earthquake.usgs.gov/earthquakes). The fatal earthquake that caused huge loss of human lives occurred in the Himalayan thrust wedge near the basal decollement which defines the lower boundary of the thrust wedge and is referred to as the Main Himalayan Thrust Fault (MHT) [1]. The three main thrust systems in the Himalayas, branching off as ramps from MHT are the Main Central thrust (MCT), Main Boundary thrust (MBT) and the Main Frontal thrust (MFT) which respectively separate the Greater Himalayan, the Lesser Himalayan, the Sub-Himalayan Zones and the Indo-Gangetic Plains from one another [2,3]. The convergence rate of Indian plate under Tibet varies from west to east along the length of the Himalayas [4]. The convergence rate across Nepal is about 20 mm/yr [5]. As a result of the fast convergence across Nepal, a portion of Himalayan thrust wedge moved southward over the Indian Plate along the MHT and resulted in the devastating earthquake on 25 April, 2015. According to the slip distribution model proposed by the "finite fault" analysis of USGS (http://earthquake.usgs.gov), a maximum slip of 3.5 m occurred. According to Zhang et al. [6], however, the slip distribution resulted in a maximum slip of 4.5 m. The main shock of 25 April was followed by more than 250 aftershocks (Fig. 1), one aftershock of *M*w6.7 occurred at depth of 22 km on 26 April, 2015 and the largest one (*M*w7.3) occurred on 12 May, 2015 with its epicentre located about 30 km east of the 25 April earthquake. The variation of earthquake magnitude with their depth of occurrence is plotted in Fig. 2.

In this paper, we have estimated and analysed the Coulomb stress change at 10 km and 15 km and 22 km depths imparted due to the earthquake based on the slip distribution model and the fault plane geometry proposed by USGS. Abundance of aftershock locations in the areas showing positive Coulomb stress change have been shown and areas experiencing positive Coulomb stress change and yet remaining devoid of any aftershock have been demarcated as probable locations for future events. The co-seismic displacement of 5 GPS stations located in Nepal after the main shock on 25 April, 2015 and the aftershock on 12 May, 2015 separately have also been estimated and analysed.

* Corresponding author.
E-mail addresses: mallika_xav@yahoo.co.in (M. Mullick), dhruba_38@yahoo.co.uk (D. Mukhopadhyay).

Peer review under responsibility of Institute of Seismology, China Earthquake Administration.

Production and Hosting by Elsevier on behalf of KeAi

http://dx.doi.org/10.1016/j.geog.2017.02.003

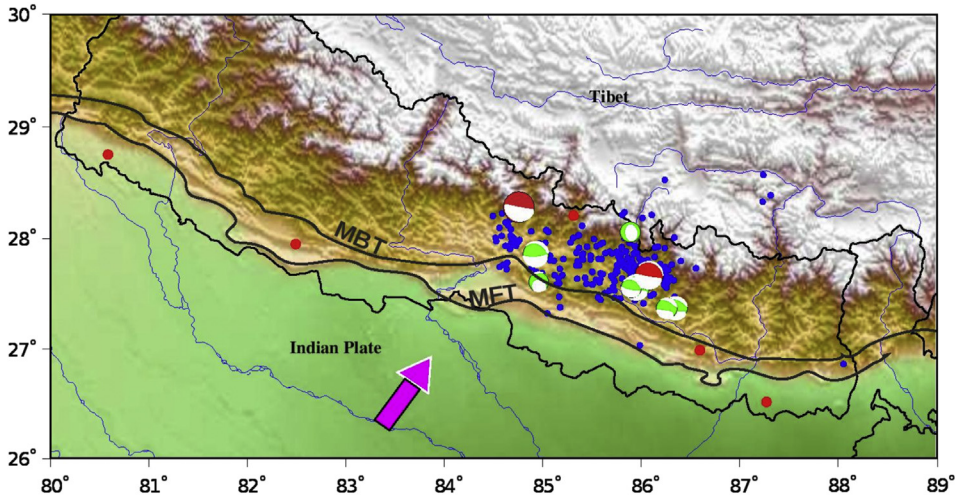

Fig. 1. Focal plane solutions of the main shock E1 and its largest aftershock E2 (red) and available focal solutions of other aftershocks (green) plotted on a topographic map of Nepal. Blue dots are epicentres of other aftershocks and red dots indicate the GPS stations. The magenta arrow shows the direction of convergence of Indian Plate under Tibet.

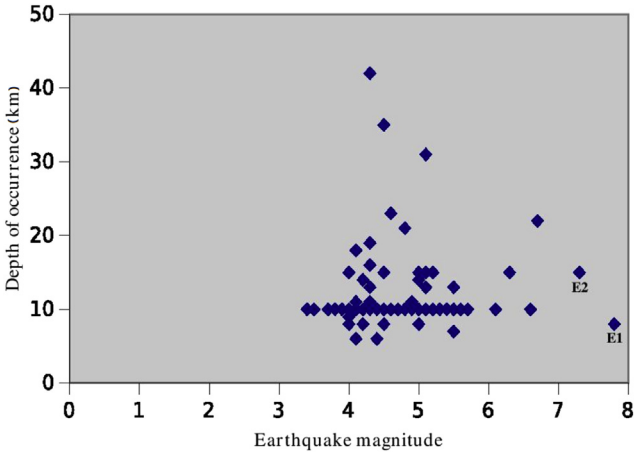

Fig. 2. Earthquake magnitude plotted against their depth of occurrence.

2. Earthquake and GPS data source and processing

Earthquake epicentre location data have been downloaded from USGS (http://earthquake.usgs.gov/earthquakes) and the focal solutions of the main event and few aftershocks have been obtained from CMT Harvard (http://www.globalcmt.org) and processed with GMT ver. 5.1.1 [7]. SOPAC Data Archive (http://sopac.ucsd.edu) has provided GPS data from 5 stations in Nepal. GPS data have been processed with GAMIT/GLOBK ver. 10.6 [8,9]. Topographic data for Fig. 1 have been obtained from http://www.ngdc.noaa.gov/mgg and Figs. 1 and 6–8 have been processed with GMT ver. 5.1.1.

3. Coulomb stress change after earthquake

3.1. Theory

Estimation and analysis of Coulomb stress change is very useful in understanding how one earthquake can trigger another as stress increase results in further earthquakes [10]. Failure of rocks in a brittle manner is a function of both shear and confining stresses formulated as Coulomb failure criterion (CFC) which is independent of regional stress but depends on fault geometry, sense of dip and co-efficient of friction. CFC requires both shear and normal stress on an incipient fault plane satisfy conditions analogous to those of friction on a pre-existing surface. Mathematically CFC is obtained from Eq. (1).

Failure occurs on a certain fault plane when the Coulomb stress σ_f exceeds the specific value given by

$$\sigma_f = \tau_\beta - \mu\left(\sigma_\beta - p\right) \tag{1}$$

where τ_β is the shear stress on the failure plane oriented at angle β with the σ_1 axis, σ_β is the normal stress, p is the pore fluid pressure and μ is the co-efficient of friction. τ_β is always taken to be positive in this expression, though in the usual process of resolution of stress τ_β can be positive or negative giving rise to right-lateral or left-lateral slip.

The Coulomb stress change (CSC) is given by Eq. (2) [11],

$$\Delta\sigma_f = \Delta\tau_\beta - \mu\left(\Delta\sigma_\beta - \Delta p\right) \tag{2}$$

Because of the tendency of Δp to counteract σ_β, the above equation is sometimes written as,

$$\Delta\sigma_f = \Delta\tau_\beta - \mu'\left(\Delta\sigma_\beta\right) \tag{3}$$

where μ' is "effective" reduced coefficient of friction given by:

$$\mu' = \mu\left(1 - \Delta p / \Delta\sigma_\beta\right) \tag{4}$$

Negative value of $\Delta\sigma_f$ in Eq. (2) would imply that failure threshold has not yet been reached, while a positive value of $\Delta\sigma_f$ would indicate that the failure threshold has been exceeded. An earthquake reduces the average value of the shear stress on the fault that slipped, but the shear stress rises at the fault tips and elsewhere also. Stress increase of less than 1.5 bar appears sufficient to trigger an earthquake and stress decrease of similar amount are sufficient to suppress them [10].

3.2. Results

The 25 April, 2015 earthquake (E1) occurred at a depth of 8.2 km when a fault plane with strike = 295°, dip = 10° slipped along MHT according to the "finite fault" analysis of USGS. The main shock E1 was followed by a large number of aftershocks (about 256) which

continued for another 20–25 days (Fig. 1). The aftershocks of E1 resulted from the failure to sustain the positive Coulomb stress change (CSC) imparted on the fault plane after the main shock while there remained many parts around the location of E1 where CSC was positive and yet no aftershock occurred in that area.

We have estimated CSC using Coulomb 3.3 software [12] on MATLAB platform due to E1 imparted on the causative fault plane at a depth of 10 km where the main shock gave rise to the maximum number of aftershocks and then at depth 15 km which hosted the largest aftershock E2 and at depth 22 km where a *M*w6.7 aftershock occurred. Following the model proposed by "finite fault" analysis of USGS the slip has been distributed on a fault plane of size 232 km × 160 km (length × width) which has been subdivided into 121 cells with the maximum slip to be 3.5 m. The USGS slip model has estimated zero slip for all the cells bordering the rectangular fault plane, and therefore, effectively the size of the thrust sheet that actually slipped is about 160 km × 115 km (length × width). The slip distribution model of USGS reports variable rake at each cell but we have assumed a mean value of 108° for all cells following Mitra et al. [13]. Coefficient of friction is taken as 0.4 which is the standard value in case of hard rocks.

Fig. 3a shows the CSC imparted due to E1 on a fault plane with strike = 295°, dip = 10° at a depth of 10 km with the aftershocks occurring at depth 10 km overlain on it. As expected, the bordering areas of the fault plane have experienced positive CSC. Since a CSC of +1.5 bar is enough to trigger $M > 5$ earthquake [10] the area marked in red (Fig. 3a) with maximum CSC (+8 bar) is the zone of greatest hazard. Fig. 3a shows that aftershocks are most abundant where CSC rose by +8 bar. But, in the southern and western fringe of the fault plane CSC is +2 to +4 bar and yet these areas have not hosted any aftershock. The cross-sectional view of CSC plotted on a vertical plane through profile AB shows good agreement of occurrence of aftershock epicentre with positive CSC (Fig. 3b).

The CSC due to E1 has been estimated on a fault plane with strike = 305°, dip = 9° and rake = 90° (Fig. 4a), which, according to USGS, hosted the largest aftershock E2 at a depth of 15 km. The location of aftershocks occurring at depth between 15 km and 20 km have been overlain on it. Most of them have occurred in the area of positive CSC including the fatal E2. The CSC plotted on a vertical plane (Fig. 4b) also confirms this consistency. The extreme southern fringe of the fault plane shows CSC to be 0 bar but just to its north and along the western fringe CSC is +2 to +4 bar where no aftershock has occurred. However, a good number of aftershocks have occurred in the area where the CSC estimated at depths 10 km and 15 km has dropped up to −7 bar as seen in Figs. 3a and 4a (blue zone). Most of these aftershocks occurred on 25 April immediately after the main shock E1. These aftershocks may have resulted from stress increase on a different fault plane at that location.

CSC due to E1 has been estimated at depth 22 km (Fig. 5a) where the aftershock of magnitude 6.7 occurred on 26, April, 2015. Fig. 5a shows that the aftershock is located where CSC is about +8 bar. Variation of CSC with depth plotted in Fig. 5b also justifies the event. Though the southern and western fringe and northern part of the fault plane have experienced CSC from +2 to +8 bar, no other major aftershock took place at 22 km depth.

Major parts of the fault plane experienced positive CSC (from +2 to +8 bar) at depths 10 km, 15 km and 22 km but no aftershock occurred in that area. The enhanced stress in these parts will probably drop in due course through future earthquakes.

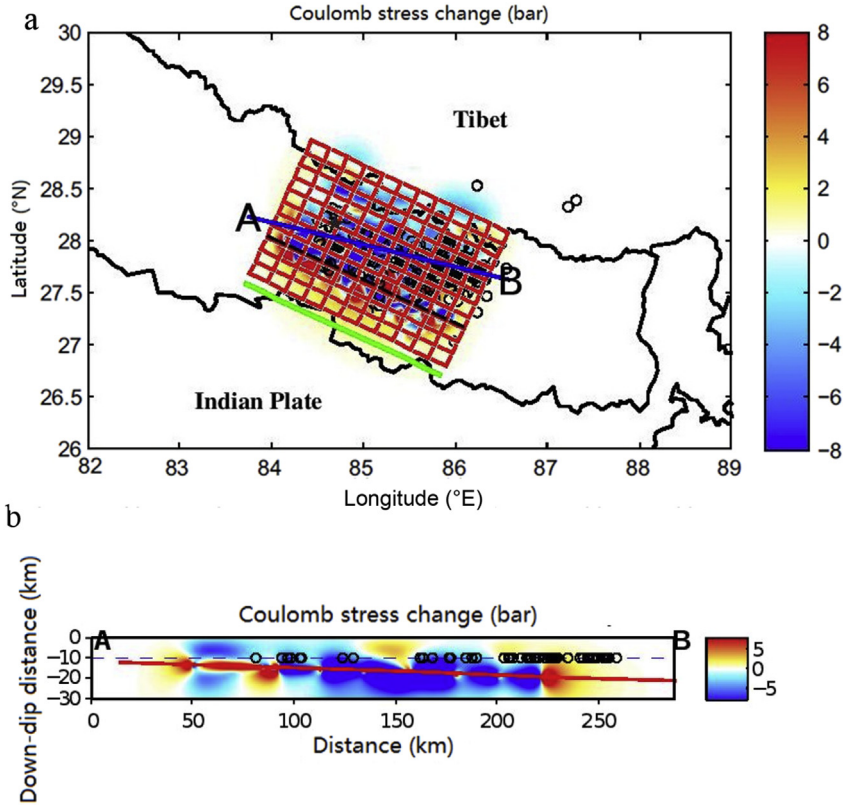

Fig. 3. a: Coulomb stress change imparted on a plane with strike = 295°, dip = 10° and rake = 108° at depth 10 km due to E1 (black star) with aftershocks of E1 (black circles) at depth 10 km overlain on the plot. Rectangular box indicates causative fault plane divided into 121 cells, green line marks the surface projection of the fault tip and black line denotes depth of stress calculation. b: Coulomb stress change on a vertical plane through profile AB (Fig. 3a) with aftershocks plotted as black circles. Red line marks the fault.

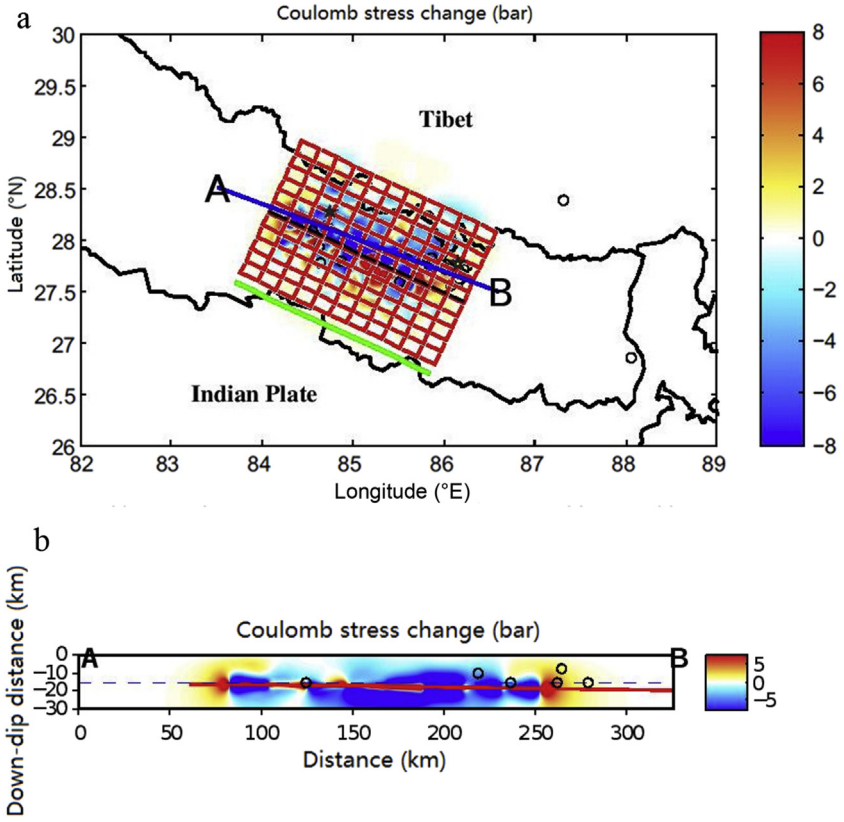

Fig. 4. a: Coulomb stress change imparted on a plane with strike = 305°, dip = 9° and rake = 90° which hosted E2 (yellow star) at depth 15 km due to E1 (black star) with aftershocks of E1 (black circles) at depth 15–20 km overlain on the plot. Green line marks the surface projection of the fault tip and black line denotes depth of stress calculation. b: Coulomb stress change on a vertical plane through profile AB (Fig. 4a) with aftershocks plotted as black circles. Red line marks the fault.

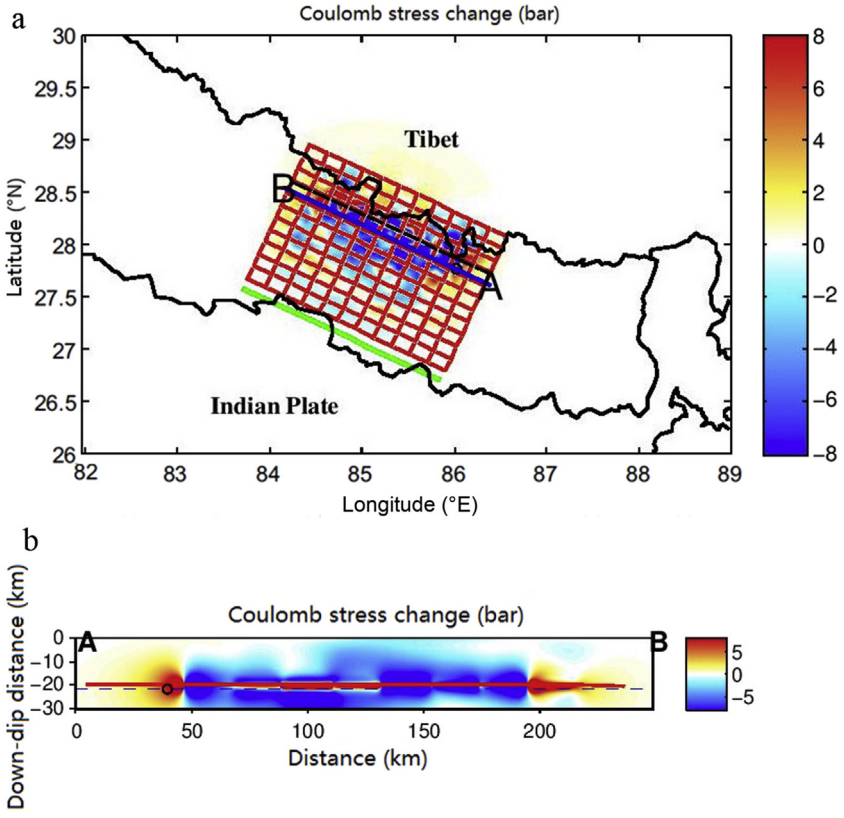

Fig. 5. a: Coulomb stress change imparted on a plane with strike = 295°, dip = 10° and rake = 108° at depth 22 km due to E1 (black star) with aftershock of *M*w6.7 (black circle) at depth 22 km overlain on the plot. Green line marks the surface projection of the fault tip and black line denotes depth of stress calculation. b: Coulomb stress change on a vertical plane through profile AB (Fig. 5a) with the aftershock plotted as black circle. Red line marks the fault.

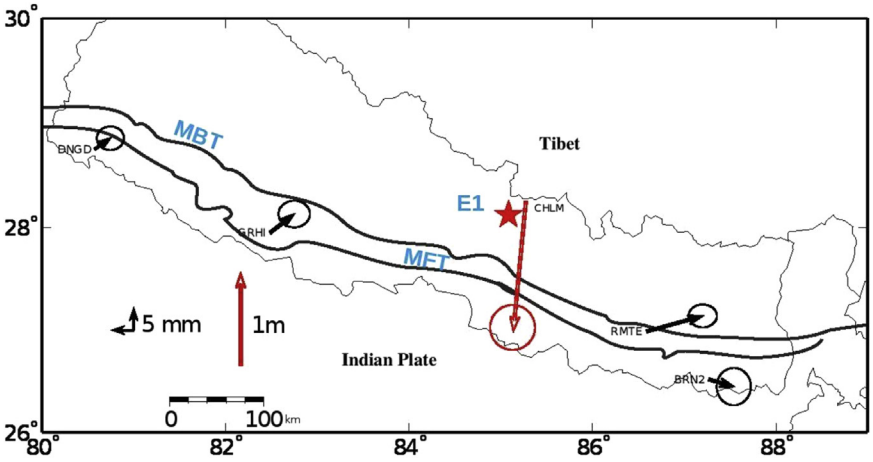

Fig. 6. Co-seismic offset of 5 GPS stations in Nepal due to E1 (red star) only.

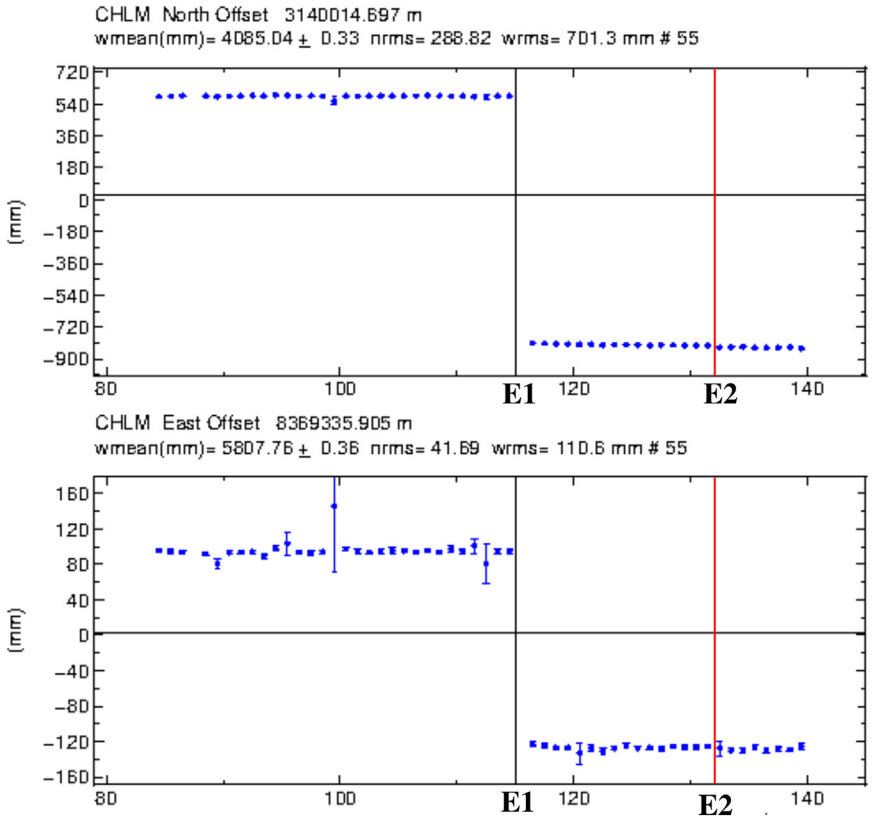

Fig. 7. Time series of north and east component of position of station CHLM which suffered maximum offset due to E1. Black vertical line denotes day of occurrence of E1 and red line denotes that of E2.

4. Co-seismic displacement of GPS stations

The focal solutions of the main events, *M*w7.8 earthquake on 25 April, 2015 (E1), aftershock of *M*w7.3 on 12 May, 2015 (E2) and the available focal solutions of the other aftershocks as shown in Fig. 1 clearly indicate pure thrust movement to be the cause of the events.

4.1. Methodology

For estimating co-seismic displacement of the 5 GPS stations in Nepal station velocities have been estimated first from data over a span of three years (March, 2013 to 30 May, 2015). Apart from these 5 stations, all the stations included in the velocity analysis are IGS stations with well determined coordinates. Hence, stations which are out of probable reach of the earthquake are kept tightly constrained while those likely to fall in the affected area are kept loosely constrained. With the velocity solution as input, a shell script given in the GLOBK suite of programs has been run to extract the co-seismic offset of these stations due to the main shock that occurred on 25 April, 2015 at 06:11: 29 UTC plus the aftershocks that followed on that day. The

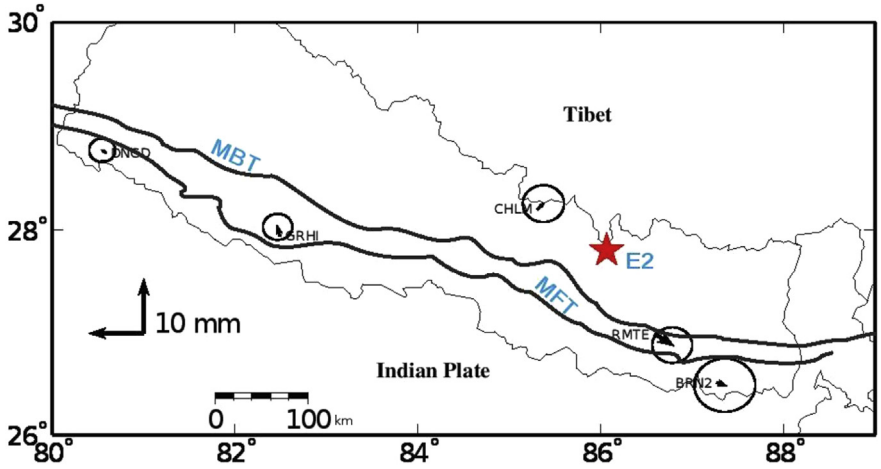

Fig. 8. Co-seismic offset of 5 GPS stations in Nepal due to E2 (red star) only.

co-seismic offset due to the largest aftershock that occurred on 12 May, 2015 is then separately extracted from the velocity solution.

4.2. Results

Co-seismic offset of 5 GPS stations in Nepal after E1 and before E2 are shown in Fig. 6. As a result of E1 only, station RMTE located south of MBT has been offset by 12.3 ± 2.0 mm towards ENE while station CHLM located north of MBT has moved southward by 1.41 ± 0.4 m. The time series of position of CHLM shown in Fig. 7 shows the huge offset in north and east components on 115th day of the year when E1 occurred. Stations DNGD and GRHI located south of MBT have been displaced in NE direction while station BRN2 located south of MFT has moved in SE direction. The southward offset of station BRN2 is ambiguous but may be justified considering the fact that GPS derived co-seismic displacement is the cumulative effect of the main shock plus the large number of aftershocks that occurred on that day. The largest aftershock of E1 was E2 (*M*w7.3) that occurred on 12 May, 2015 with epicentre located 30 km east of E1. The co-seismic displacement of the 5 GPS stations in Nepal due to E2 only have been extracted from the velocity solution and plotted in Fig. 8. Stations, including CHLM located nearest to the epicentre of E2, do not show remarkable offset due to E2 alone. Time series of CHLM in Fig. 7 also does not indicate major displacement on the 132nd day of 2015 when E2 took place.

5. Conclusions

On 25 April, 2015 a southward slip on about 160 km × 115 km portion of MBT resulted in the devastating earthquake of *M*w7.8 (E1) in Nepal and the largest aftershock of *M*w7.3 (E2) on 12 May, 2015 and killed thousands of human lives and left many injured and homeless. GPS stations DNGD, GRHI and RMTE situated south of MBT have moved in the northeast direction and among these three stations RMTE has experienced the maximum offset of 12.3 ± 2.0 mm towards ENE. while station CHLM located in the higher Himalayas north of MBT has been offset by 1.41 ± 0.4 m southward due to E1. The co-seismic offset of GPS stations due to E2 alone are not remarkable.

The main shock of 25 April was followed by about 256 aftershocks resulting from the failure to sustain the positive Coulomb stress change imparted at various depths due to the main event. The locations of greater number of aftershocks at 10 km depth are consistent with the Coulomb stress change imparted at depth of 10 km on a fault plane with strike = 295°, dip = 10° and rake = 108°. The locations of aftershocks of magnitude >5 including the largest event of *M*w7.3 on 12 May, 2015 (E2) are consistent with Coulomb stress change imparted on a fault plane with strike = 305°, dip = 9° and rake = 90° at depth of 15 km. The aftershock of *M*w6.7 at depth 22 km which occurred on 26, April, 2015 agrees well with the CSC estimated at that depth. But the stress increase that resulted from the E1 event has not been released totally through aftershocks. The main shock E1 has resulted in generating positive CSC at depths 10 km, 15 km and 22 km in the bordering parts of the fault plane without any aftershock occurring there. The accumulating stress will probably be released in the coming decades. Therefore these regions of enhanced CSC should be treated as future threats for the people of Nepal.

Acknowledgement

Mallika Mullick wishes to thank Department of Science & Technology and Dhruba Mukhopadhyay wishes to thank INSA Honorary Scientist Project for financial support.

References

[1] L.D. Brown, W. Zhao, K.D. Nelson, M. Hauck, D. Alsdorf, A. Ross, et al., Bright spots, structure, and magmatism in southern Tibet from INDEPTH seismic reflection profiling, Science 274 (1996) 1688–1690.
[2] K.V. Hodges, Tectonics of the Himalayas and southern Tibet from two perspectives, Geol. Soc. Am. Bull. 112 (2000) 324–350.
[3] A. Yin, Cenozoic tectonic evolution of the Himalayan orogen as constrained by along-strike variation of structural geometry, exhumation history and foreland sedimentation, Earth Sci. Rev. 76 (1) (2006) 1–131.
[4] P. Banerjee, R. Burgmann, B. Nagarajan, E. Apel, Intraplate deformation of the Indian subcontinent, Geophys. Res. Lett. 35 (2008) L18301.
[5] R. Bilham, K. Larson, J. Freymueller, Project Idylhim Members, GPS measurements of present day convergence across the Nepal Himalaya, Nature 386 (1997) 61–64.
[6] G. Zhang, E. Hetland, X. Shan, Slip in the 2015 *M*w 7.9 Gorkha and *M*w 7.3 Kodari, Nepal earthquakes revealed by seismic and geodetic data: delayed slip in the Gorkha and slip deficit between the two earthquakes, Seismol. Res. Lett. 86 (6) (2015) 1578–1586.
[7] P. Wessel, W.H.F. Smith, R. Scharro, J.F. Luis, F. Wobbe, Generic mapping tools: improved version released, EOS Trans. AGU 94 (45) (2013).
[8] T.A. Herring, R.W. King, S.C. McClusky, GAMIT Reference Manual, Release 10.6, Department of Earth, Atmosphere and Planetary Sciences, M.I.T, Cambridge, 2015a.
[9] T.A. Herring, R.W. King, S.C. McClusky, Global Kalman Filter VLBI and GPS Analysis Program, Documentation, Release 10.6, Department of Earth, Atmosphere and Planetary Sciences, M.I.T, Cambridge, 2015b.

[10] G.C.P. King, R.S. Stein, J. Lin, Static stress changes and the triggering of earthquakes, Bull. Seismol. Soc. Am. 84 (1994) 935–953.
[11] R.S. Stein, The role of stress transfer in earthquake occurrence, Nature 402 (1999) 605–609.
[12] S. Toda, R.S. Stein, V. Sevilgen, J. Lin, Coulomb 3.3 Graphic-Rich Deformation and Stress Change Software for Earthquake, Tectonic and Volcano Research and Teaching – User Guide: U.S. Geological Survey Open-File Report 2011-1060, 2011.
[13] S. Mitra, H. Paul, A. Kumar, S.K. Singh, S. Dey, D. Powali, The 25 April 2015 Nepal earthquake and its aftershocks, Curr. Sci. 108 (10) (2015) 1938–1943.

Mallika Mullick, works in Raman Centre for Applied and Interdisciplinary Sciences, 16A, Jheel Road, Kolkata-700075, India. E-mail: mallika_xav@yahoo.co.in.